Location-Aware UWB Communication with Generalized Energy Detection Receivers

Heinrich Luecken, *Student Member, IEEE,* Christoph Steiner, and Armin Wittneben, *Member, IEEE*

***Abstract*—Future wireless networks based on Ultra-Wideband (UWB) will offer localization capabilities with centimeter accuracy. We propose to use this inherently obtainable location knowledge to adapt the transceiver to the multipath channel conditions. This saves overhead for channel estimation and dissemination and enables low cost, low complexity and low power data transmission. In particular, we study the location-aware adaptation of generalized energy detection receivers for UWB impulse radio communication with binary pulse position modulation. Conventionally, these receivers are very vulnerable to narrowband interference. Therefore, we derive transmitter and receiver optimization schemes based on the Signal-to-Interference-plus-Noise-Ratio (SINR): First, we present the SINR optimization based on full channel knowledge. The location knowledge is then incorporated by means of a statistical channel model, which depends on the position of the nodes. Performance evaluation based on a simple channel model is used to give insight about the fundamental behavior of the derived optimization schemes. Moreover, an extensive measurement campaign in a rich scattering environment proves that location information can improve the data transmission and helps to successfully suppress narrowband interference. Performance gains of 2 to 5 dB compared to conventional energy detection can be obtained.**

***Index Terms*—Ultra-Wideband, low complexity, impulse radio, generalized energy detection receiver, narrowband interference, SINR optimization.**

I. Introduction

LOCATION information is one of the key enablers for emerging applications of wireless sensor networks (WSN) and body area networks (BAN). For many applications, joint localization and data communication is desirable, e.g. tracking items in a production hall, airport or hospital, combined with sensor data querying. If the location information is available, it can be used for performance enhancement of data transmission. So far, this approach has been investigated for higher layers such as routing [1] or security protocols [2]. We propose to use the location information on the physical layer to improve the performance of low complexity and low data rate UWB communication.

The key requirements of WSN and BAN are low cost, small form factor and low energy consumption [3], [4]. UWB communication offers a versatile design space to meet these design goals. This is the consequence of a paradigm shift compared to narrowband communication: Due to the huge bandwidth available, we can trade off bandwidth efficiency against other figures of merit. In fact, there is a growing interest in receivers that sacrifice detection performance for a very cheap implementation [5]. With an available bandwidth of up to 7.5 GHz in the band from 3.1 to 10.6 GHz, the major design criterion is not data rate anymore, but rather power consumption and hardware complexity. The high bandwidth of UWB makes it difficult to obtain full knowledge of the multipath channel (particularly at the transmitter) and conventional approaches may require very high-speed analog-to-digital conversion. This leads to hardware-aware system designs and motivates the use of impulse radio (IR) and noncoherent receiver structures [6]. Within the group of noncoherent receivers, the generalized energy detector is of particular relevance. It can be efficiently implemented in analog hardware as it merely consists of a squarer and a low-pass filter. Nevertheless, it shows reasonable detection performance. As bandwidth efficiency is of minor importance, binary modulation schemes are preferable due to their robustness. We thus focus on the generalized energy detector receiver with binary pulse position modulation (BPPM) in this paper. Specifically we introduce location-aware precoding schemes and study the location-aware post-detection filter adaptation, both of which with the intention to improve the bit error rate (BER) performance and the robustness against narrowband interference.

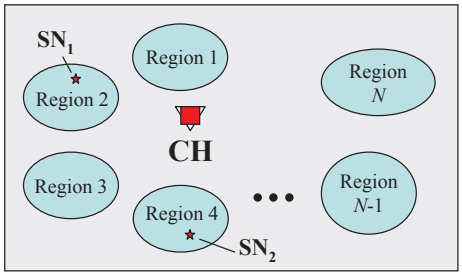

Fig. 1. Network scenario with a cluster head (CH), sensor nodes (SN), and regions $1, \ldots, N$.

As an example, let us consider the following scenario: As shown in Fig. 1, the coverage area of a network might be divided into N subregions. We consider a heterogeneous network with very low complexity UWB sensor nodes (SN). These reduced function devices communicate with stationary cluster heads (CH), which are full-function devices with less stringent complexity constraints. The downlink (CH to SNs) is the bottleneck in this scenario since the SNs are of low

Manuscript received January 17, 2011; revised September 21, 2011 and February 2, 2012; accepted May 18, 2012. The associate editor coordinating the review of this paper and approving it for publication was L. Yang.

H. Luecken and A. Wittneben are with the Communication Technology Laboratory, ETH Zurich, 8092 Zurich, Switzerland (e-mail: {lueckenh, wittneben}@nari.ee.ethz.ch).

C. Steiner was with the Communication Technology Laboratory, ETH Zurich. He is now with Infineon Technologies Austria AG, 8010 Graz, Austria (e-mail: christoph.steiner@infineon.com).

Digital Object Identifier 10.1109/TWC.2012.070912.110101

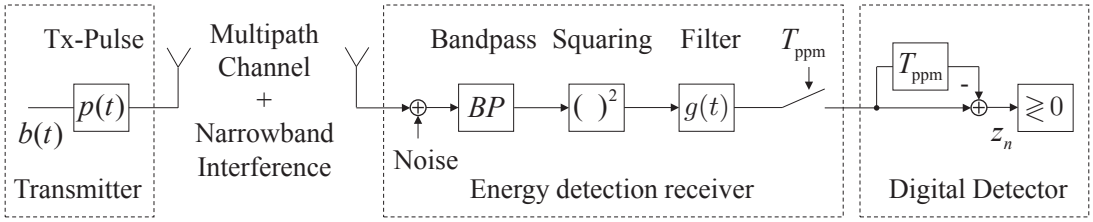

Fig. 2. Block diagram of transmitter, channel and receiver.

complexity and achieve a lower receiver sensitivity than the CH. Therefore, we consider the optimization of the downlink data transmission in the following discussion.

Conventional approaches attempt to adapt the transceiver directly to the channel state. They require the knowledge of the channel state over the full transmission bandwidth. Due to the huge bandwidth of UWB, the estimation and dissemination of channel state information (CSI) requires high complexity and is very expensive and power hungry. To circumvent this problem, we propose to adapt the transceiver to the region of the SN. This is done by modeling the channel impulse response as a random process with region dependent parameters, which can be estimated in an off-line training phase. The data transmission is then optimized based on the statistical channel knowledge for each region. This is the key to location-aware communication. The CHs are able to determine the region, in which a SN is located. This can for example be accomplished by location fingerprinting techniques [7]. Based on the statistical channel knowledge for each region, we propose two different approaches to improve the data transmission:

- Transmitter optimization at CH: The CH uses a region specific transmit signal depending on where the SN is located. This approach uses a fixed post-detection filter receiver at the SN and applies precoding at the CH according to the channel statistics of the region.
- Receiver optimization at SN: This approach uses adaptable post-detection filters at the SN. The CH feeds back the region number to the SN and based on the regional channel statistics the SN can adapt the post-detection filter.[1]

Both approaches improve the detection performance and can be used to successfully suppress the influence of narrowband interference.

Fig. 2 shows the system model which we will use throughout the paper. The transmitter uses BPPM, i.e.

$$b(t) = \sum_n c_n \delta(t - a_n T_{\text{ppm}} - nT_{\text{symb}}).$$

For transmission of symbol $a_n = 0$, a pulse $p(t)$ is sent in the first time slot and for a "1", it is sent in the second time slot. The length of the time slot T_{ppm} is half the symbol duration T_{symb}. The polarity c_n of the pulses is chosen randomly to avoid discrete spectral lines in the spectrum of the transmit signal. The generalized energy detector consists of a bandpass filter of bandwidth B and center frequency f_c, a squaring device and the post-detection filter with impulse response $g(t)$. Data detection is based on two samples per symbol taken at the energy detector output. The energy in the first time slot is compared to the energy in the second time slot.

If the post-detection filter has a rectangular impulse response (sliding window integrator), the generalized energy detection receiver corresponds to a conventional energy detector. It may however be preferable to use other filters. In terms of hardware complexity and power consumption, a simple first order low-pass filter outperforms the sliding window integrator. See [8] for details. In terms of detection performance, the post-detection filter can be adapted to the channel conditions and the narrowband interference scenario.

In this paper we study the location-aware optimization of either $p(t)$ or $g(t)$. The contribution can be summarized as follows:

- We derive an explicit expression for the Signal-to-Interference-plus-Noise-Ratio (SINR) for the generalized energy detection receiver as a function of the transmit pulse (Proposition 1) and the post-detection filter (Proposition 2), see Section III.
- Optimization algorithms for the transmitter and receiver are deduced (Section IV). As reference we first study a scenario in which full CSI is available for the optimization. Subsequently, we relax this condition and assume that only location (region) specific statistical CSI is available. We use a BER criterion as cost function for the optimization of $g(t)$ and $p(t)$ and introduce some approximations that reduce the computational complexity.
- The performance of the proposed schemes is investigated on the basis of channel models and channel measurements (Section V).

Related Work: A comprehensive overview on UWB communications is given in [5] and an overview on noncoherent UWB in [6]. To the best of the authors knowledge, precoding for UWB generalized energy detection receivers has so far not been considered in literature. In [9] and [10], the authors of this paper have published some early results (mSINR and mLSA) that turn out to be special cases of the overall framework, which is introduced here. Transmitter optimization and pulse shaping for coherent receivers has been extensively studied in literature, e.g. [11]–[13]. Common objectives are spectral mask, bit error rate [11] or multiuser performance [12] as well as narrowband interference suppression for linear receivers [13]. For low-complexity receivers, time-reversal prefiltering [14]–[16] and channel-phase-precoded (CPP) UWB [17], [18] have been proposed. In [19], pre-equalization with spectral mask constraints is presented. Even though these

[1]The optimization can be performed at the CH or off-line in advance and then disseminated to the SNs.

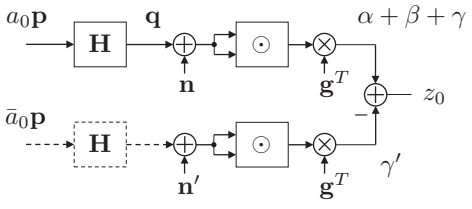

Fig. 3. Discrete time signal model.

precoding methods are related to the one we propose in this paper, they neither suppress narrowband interference nor are they suitable for generalized energy detection receivers. With regard to receiver optimization, our work is related to [20]–[23]. In [20], the ML decision rule based on the average PDP of the channel impulse response is derived and [22] presents ML detectors with partial CSI and intersymbol interference. Ref. [23] evaluates the performance of these receivers in a body area environment. In [21], energy detection with multiple energy measurements is studied. However, compared to the approaches reported in literature, we take also narrowband interference into account and explicitly impose a low receiver complexity constraint.

Notation: Boldface lowercase and uppercase letters indicate column vectors and matrices, respectively. $(\cdot)^T$, $\odot$, $\mathsf{E}[\cdot]$ and $\nabla_{\mathbf{x}}(\cdot)$ denote transposition, Hadamard product, expectation, and gradient with respect to $\mathbf{x}$, respectively. The principle eigenvector is denoted by $\mathbf{v}_{\max}\{\cdot\}$ and for the generalized eigenvalue problem by $\mathbf{v}_{\max}\{\cdot,\cdot\}$.

II. System Model

In the following, we look at the transmission of a single symbol $a_0 \in \{0,1\}$. The considered transmission scheme can be modeled in discrete time[2] and vector notation as depicted in Fig. 3. The upper branch corresponds to the first time slot and the lower branch to the second time slot.

The transmit pulse is denoted by $\mathbf{p} \in \mathbb{R}^N$ and the receive pulse is then given by $\mathbf{q} = \mathbf{H}\mathbf{p}$. The channel matrix $\mathbf{H}$ includes the bandpass filter and has a Toeplitz structure with dimensions $N \times N$. It collects the shifted and zero-padded versions of the band-pass filtered channel impulse response $[h[1], h[2], \ldots, h[N_h], 0, \ldots, 0]^T$ on its columns, where N_h times the sampling period denotes the channel excess delay. Thermal noise plus narrowband interference are modeled as zero-mean Gaussian random vectors $\mathbf{n}$ (first time slot) and $\mathbf{n}'$ (second time slot). Their covariance matrices including the band-pass filter are given by

$$\mathbf{\Sigma}_{nn} = \mathsf{E}[\mathbf{n}\mathbf{n}^T] = \mathsf{E}[\mathbf{n}'\mathbf{n}'^T] = \mathbf{\Sigma}_{\tilde{w}} + \mathbf{\Sigma}_{\tilde{i}},$$
$$\mathbf{\Sigma}_{n'n} = \mathsf{E}[\mathbf{n}\mathbf{n}'^T] = \mathsf{E}[\mathbf{n}'\mathbf{n}^T]^T.$$

$\mathbf{\Sigma}_{\tilde{w}}$ and $\mathbf{\Sigma}_{\tilde{i}}$ denote the covariance matrix of the band-limited noise and interference, respectively. For notational convenience, the impulse response of the post-detection filter is stacked into a vector in reverse order, i.e. $\mathbf{g} = (g[N], g[N-1], \ldots, g[1])^T$. The matrix $\mathbf{G} = \mathrm{diag}(\mathbf{g})$ carries these values on the main diagonal.

[2]Note that this sampling is only necessary for the theoretical analysis. The receiver implementation is in analog without any high rate sampling.

This system model is equivalent to the continuous time transceiver structure depicted in Fig. 2 under the following assumptions:

- The sampling period T_s must fulfill at least $\frac{1}{T_s} \geq 2B + 4f_c$ to account for the squaring operation.
- Edge effects due to the finite length of the signals are negligible.
- Intersymbol interference can be neglected, i.e., $\int_{-\infty}^{\infty} g(\tau)q^2(t-\tau)d\tau = 0$ for $t \notin [0, T_{\text{ppm}}]$, where $q(t)$ denotes the received pulse. This condition is fulfilled if the channel excess delay plus the time duration of the transmit pulse and impulse response of the post-detection filter is smaller than the PPM half slot T_{ppm}. This is a reasonable assumption in our context, because in sensor networks the per node peak data rate is moderate.
- Narrowband interference is Gaussian distributed.
- The transmit bits are equally probable and only one pulse is transmitted per symbol with perfect synchronization at the receiver.[3]

III. Signal-to-Interference-and-Noise Ratio

The Signal-to-Interference-and-Noise Ratio (SINR) is defined as

$$\mathrm{SINR} = \frac{\mathsf{E}[z_0|a_0=0]^2}{\mathsf{Var}[z_0|a_0=0]} = \frac{\mathsf{E}[z_0|a_0=1]^2}{\mathsf{Var}[z_0|a_0=1]}, \qquad (1)$$

where z_0 denotes the receiver output and expectation is with respect to noise and interference. Conditioned on the transmit symbol, the SINR corresponds to the squared mean of the decision variable over its variance. Since the mean and the variance are the same for both transmit symbols and they occur with equal probability, the SINR is independent of the transmit symbol. Therefore, in the following we will consider only the case that the pulse is in the first time-slot, i.e. $a_0 = 0$. The decision variable z_0 is then given by

$$z_0|_{a_0=0} = \mathbf{g}^T\left[(\mathbf{q}+\mathbf{n}) \odot (\mathbf{q}+\mathbf{n})\right] - \mathbf{g}^T\left[\mathbf{n}' \odot \mathbf{n}'\right]. \qquad (2)$$

Expanding the squares leads to

$$\underbrace{\mathbf{g}^T(\mathbf{q}\odot\mathbf{q})}_{=:\alpha} + \underbrace{2\mathbf{g}^T(\mathbf{q}\odot\mathbf{n})}_{=:\beta} + \underbrace{\mathbf{g}^T(\mathbf{n}\odot\mathbf{n}) - \mathbf{g}^T(\mathbf{n}'\odot\mathbf{n}')}_{=:\gamma}.$$

The term α collects the desired signal contribution, i.e. the receive pulse $\mathbf{q}$, which is squared and convolved with the post-detection filter. All perturbing contributions are combined in the other terms: in β the product of the signal and the noise plus interference, and in γ the squared noise plus interference contribution of the first and second timeslot, respectively.

The SINR can then be written in terms of the squared signal, the mixed term and the squared noise term as follows:

$$\mathrm{SINR} = \frac{\mu_\alpha^2}{\sigma_\beta^2 + \sigma_\gamma^2}$$

The numerator μ_α^2 equals the desired squared signal contribution α and the denominator is given by the variance σ_β^2 of the mixed signal and interference plus noise term and the variance σ_γ^2 of the squared noise and interference γ.

[3]Synchronization for this receiver structure has been considered in [24].

This signal structure at the energy detector output leads to the particular characteristic of this receiver structure. On the one hand, the squared terms are not Gaussian distributed anymore and can be shaped by the choice of the post-detection filter. On the other hand, the mixed term β depends on the transmit pulse as well. This enables distinct features of transmitter optimization, e.g. specific transmit pulse shapes for interference suppression.

Proposition 1: The SINR in terms of the transmit pulse $\mathbf{p}$ is given by

$$\mathrm{SINR} = \frac{\left(\mathbf{p}^T\mathbf{A}\mathbf{p}\right)^2}{\mathbf{p}^T\mathbf{B}_\beta\mathbf{p} + \sigma_\gamma^2}, \tag{3}$$

where

$$\begin{aligned}\mathbf{A} &= \mathbf{H}^T\mathbf{G}\mathbf{H},\\ \mathbf{B}_\beta &= 4\mathbf{H}^T\mathbf{G}\boldsymbol{\Sigma}_{nn}\mathbf{G}^T\mathbf{H},\\ \sigma_\gamma^2 &= 4\mathbf{g}^T\left(\boldsymbol{\Sigma}_{nn}\odot\boldsymbol{\Sigma}_{nn} - \boldsymbol{\Sigma}_{n'n}\odot\boldsymbol{\Sigma}_{n'n}\right)\mathbf{g}.\end{aligned}$$

Proof of Proposition 1: See Appendix A.

Proposition 2: The SINR in terms of the post-detection filter $\mathbf{g}$ is given by

$$\mathrm{SINR} = \frac{\mathbf{g}^T\mathbf{K}\mathbf{g}}{\mathbf{g}^T\mathbf{C}\mathbf{g}} \tag{4}$$

where

$$\begin{aligned}\mathbf{K} &= \mathbf{H}\mathbf{p}\mathbf{p}^T\mathbf{H}^T \odot \mathbf{H}\mathbf{p}\mathbf{p}^T\mathbf{H}^T\\ \mathbf{C} &= 4\left(\mathbf{H}\mathbf{p}\mathbf{p}^T\mathbf{H}^T\odot\boldsymbol{\Sigma}_{nn} + \boldsymbol{\Sigma}_{nn}\odot\boldsymbol{\Sigma}_{nn} - \boldsymbol{\Sigma}_{n'n}\odot\boldsymbol{\Sigma}_{n'n}\right).\end{aligned}$$

Proof of Proposition 2: See Appendix B.

IV. Optimization of Transmitter or Receiver

This section presents optimization algorithms based on the SINR expressions that have been derived in Section III. First, we present the optimization of the transmit pulse $\mathbf{p}$ and post-detection filter $\mathbf{g}$ for a given channel realization. This provides performance bounds for the generalized energy detection receiver. Such a transmission scheme requires the full knowledge of the channel impulse response at the transmitter and/or receiver, which might be expensive to obtain and might require a lot of overhead. Hence, in the second part of this section, we present optimization schemes based on statistical channel knowledge, i.e. the covariance matrix of the channel impulse response to incorporate the location knowledge.

A. Full channel knowledge

Transmitter Optimization: Given a certain post-detection filter, the optimization problem for the transmit pulse can be formulated as follows:

$$\mathbf{p}^* = \underset{\mathbf{p}\in\mathbb{R}^N:\|\mathbf{p}\|=1}{\arg\max}\ \mathrm{SINR} \tag{5}$$

The maximization is subject to a norm constraint on $\mathbf{p}$, i.e. the energy per bit is limited. For environments where the FCC regulation [25] is applied, the given constraint is an approximation on the peak level of emissions[4]. Since the scope of this paper is on low data rate systems, the average power constraint[5] is without effect [6]. However, to extend the optimization to high data rate systems, the average power constraint could also be included, e.g. as presented in [19]. Optionally, the transmit pulse must be scaled to be compliant with the regulation.

Using the substitution $\mathbf{p} = \tilde{\mathbf{p}}/\|\tilde{\mathbf{p}}\|$, the transmit power constraint is fulfilled for all $\tilde{\mathbf{p}}$. With (3) from Proposition 1, we can write (5) then as an unconstrained optimization problem

$$\mathbf{p}^* = \underset{\tilde{\mathbf{p}}\in\mathbb{R}^N}{\arg\max}\ \frac{\left(\tilde{\mathbf{p}}^T\mathbf{A}\tilde{\mathbf{p}}\right)^2}{\tilde{\mathbf{p}}^T\mathbf{B}\tilde{\mathbf{p}}\cdot\tilde{\mathbf{p}}^T\tilde{\mathbf{p}}}, \tag{6}$$

where

$$\begin{aligned}\mathbf{B} =& 4\mathbf{H}^T\mathbf{G}\boldsymbol{\Sigma}_{nn}\mathbf{G}^T\mathbf{H}\\ &+ 4\left(\mathbf{g}^T\left(\boldsymbol{\Sigma}_{nn}\odot\boldsymbol{\Sigma}_{nn} - \boldsymbol{\Sigma}_{n'n}\odot\boldsymbol{\Sigma}_{n'n}\right)\mathbf{g}\right)\mathbf{I}.\end{aligned}$$

Standard numerical algorithms can be used to solve this optimization problem, e.g. algorithms based on Newton's method. Appendix C provides the gradient and Hessian matrix of the objective function with respect to $\tilde{\mathbf{p}}$. Numerical experiments[6] show that randomly chosen starting vectors $\tilde{\mathbf{p}}_0$ always converge to the same maximum. Hence, we conjecture that the optimization is generally independent of the starting vector.

Low SINR Approximation (LSA): Depending on the operating regime of the receiver, the influence of the mixed signal and interference plus noise component and squared interference plus noise component is different. If the received signal power is high, the mixed term dominates in the denominator of the SINR expression. However, for a rather low SINR, which is the operating regime of typical UWB-IR communication, the squared interference plus noise is much larger than the mixed term, i.e. $\sigma_\beta^2 \ll \sigma_\gamma^2$. If the mixed term is neglected, the denominator of the SINR is independent of the transmit pulse shape. This assumption leads to an interesting approximation of the transmitter optimization problem:

$$\begin{aligned}\mathbf{p}_{\mathrm{LSA}}^* &= \underset{\mathbf{p}\in\mathbb{R}^N:\|\mathbf{p}\|=1}{\arg\max}\ \frac{\left(\mathbf{p}^T\mathbf{H}^T\mathbf{G}\mathbf{H}\mathbf{p}\right)^2}{4\mathbf{g}^T\left(\boldsymbol{\Sigma}_{nn}\odot\boldsymbol{\Sigma}_{nn} - \boldsymbol{\Sigma}_{n'n}\odot\boldsymbol{\Sigma}_{n'n}\right)\mathbf{g}}\\ &= \underset{\tilde{\mathbf{p}}\in\mathbb{R}^N}{\arg\max}\ \frac{\tilde{\mathbf{p}}^T\mathbf{A}\tilde{\mathbf{p}}}{\tilde{\mathbf{p}}^T\tilde{\mathbf{p}}}.\end{aligned} \tag{7}$$

The solution of (7) is given by the principal eigenvector of $\mathbf{A}$, i.e. $\mathbf{p}_{\mathrm{LSA}}^* = \mathbf{v}_{\max}\{\mathbf{A}\}$, [10].

Receiver Optimization: Considering now the post-detection filter, the optimization problem for a fixed transmit pulse can be written as:

$$\mathbf{g}^* = \underset{\mathbf{g}\in\mathbb{R}^N}{\arg\max}\ \mathrm{SINR} = \underset{\mathbf{g}\in\mathbb{R}^N}{\arg\max}\ \frac{\mathbf{g}^T\mathbf{K}\mathbf{g}}{\mathbf{g}^T\mathbf{C}\mathbf{g}} \tag{8}$$

Using Proposition 2, the SINR is written as the fraction of two quadratic forms, i.e. the solution to (8) is given by $\mathbf{g}^* = \mathbf{v}_{\max}\{\mathbf{K}, \frac{1}{2}(\mathbf{C}+\mathbf{C}^T)\}$, [26].

[4]The peak power is restricted to 0 dBm after filtering with 50 MHz centered at the frequency with the highest emission.

[5]The average power is restricted to -41.3 dBm/MHz contained on a 1 MHz band when averaged over 1 ms.

[6]We preformed the optimization for $N_h = 100$ different channel realizations and observed that the convergence is independent of the starting vector, which was randomly initialized 1000 times each.

B. Statistical channel knowledge

To avoid channel estimation at the low complexity receiver, we propose to identify the multipath conditions from the location of the SN. However, localization of SNs is always subject to estimation errors and only possible up to a certain accuracy. This requires robust optimization algorithms that do not depend on an individual channel realization but rather on the statistics of the channel conditions at a certain position. Hence, we propose to model the channel impulse response as a nonstationary random process and derive the optimization algorithms in the following.

Minimization of mean BER (mBER): Since the SINR is now a random variable, it is not anymore reasonable to maximize its value. Instead, we minimize the mean bit error probability P_e to achieve the best performance on average, i.e.

$$\mathbf{p}^*_{\text{mBER}} = \underset{\mathbf{p}\in\mathbb{R}^N:\|\mathbf{p}\|=1}{\arg\min} \ \mathsf{E}_h\left[P_e\right] \tag{9}$$

or

$$\mathbf{g}^*_{\text{mBER}} = \underset{\mathbf{g}\in\mathbb{R}^N}{\arg\min} \ \mathsf{E}_h\left[P_e\right],$$

for the transmitter or post-detection filter, respectively. The expectation is taken with respect to the channel impulse response $[h[1], h[2], \ldots, h[N_h]]^T$. However, due to the nonlinear receiver processing, a closed form expression for P_e is difficult to obtain[7]. In order to keep the problem tractable, we approximate the energy detector output as Gaussian distributed. The validity of this assumption for a similar problem has been investigated in [28]. With the Gaussian assumption, the bit error probability P_e simplifies to $P_e \approx \mathrm{Q}\left(\sqrt{\mathrm{SINR}}\right)$. To compute the mean of P_e over the channel realizations, we propose to apply Monte Carlo Integration:

$$\mathsf{E}_h\left[P_e\right] \approx \frac{1}{M_h}\sum_{i=1}^{M_h} \mathrm{Q}\left(\sqrt{\mathrm{SINR}_i}\right), \tag{10}$$

where SINR_i is computed with the ith realization of M_h randomly drawn channels according to the distribution of the channel.

To minimize the mean bit error probability, we propose to use optimization algorithms based on Newton's method. The gradient of (10) is given by

$$\nabla_{\mathbf{x}}\mathsf{E}_h\left[P_e\right] \approx \frac{1}{M_h}\sum_{i=1}^{M_h} -\frac{e^{-\frac{\mathrm{SINR}_i}{2}}}{\sqrt{8\pi\mathrm{SINR}_i}}\nabla_{\mathbf{x}}\mathrm{SINR}_i, \tag{11}$$

where $\mathbf{x}$ is either $\tilde{\mathbf{p}}$ or $\mathbf{g}$. The Hessian matrix computes to

$$H_{\mathbf{x}}\ \mathsf{E}_h\left[P_e\right] \approx \frac{1}{M_h}\sum_{i=1}^{M_h} \xi_i \cdot H_{\mathbf{x}}\ \mathrm{SINR}_i + \psi_i \cdot \nabla_{\mathbf{x}}\mathrm{SINR}_i \left(\nabla_{\mathbf{x}}\mathrm{SINR}_i\right)^T, \tag{12}$$

where

$$\xi_i = -\frac{1}{2\sqrt{2\pi\mathrm{SINR}_i}}\cdot e^{-\frac{\mathrm{SINR}_i}{2}}$$
$$\psi_i = \frac{1}{4\sqrt{2\pi}}(\mathrm{SINR}_i^{-\frac{3}{2}} + \mathrm{SINR}_i^{-\frac{1}{2}})\cdot e^{-\frac{\mathrm{SINR}_i}{2}}.$$

Since $\mathsf{E}_h\left[P_e\right]$ may have many local minimums, we cannot guarantee to find the optimal solution. However, in the following we will describe two approximations that can serve as starting vectors for the iterative solution of the optimization problem.

Maximization of mean SINR *(mSINR)*: As an alternative to (9), the optimization can be performed with respect to the mean signal and mean interference plus noise power, i.e. for the transmitter

$$\begin{aligned}\mathbf{p}^*_{\text{mSINR}} &= \underset{\tilde{\mathbf{p}}\in\mathbb{R}^N}{\arg\max}\ \frac{\mathsf{E}_h\left[\tilde{\mathbf{p}}^T\mathbf{A}\tilde{\mathbf{p}}\right]^2}{\mathsf{E}_h\left[\tilde{\mathbf{p}}^T\mathbf{B}\tilde{\mathbf{p}}\cdot\tilde{\mathbf{p}}^T\tilde{\mathbf{p}}\right]}\\ &= \underset{\tilde{\mathbf{p}}\in\mathbb{R}^N}{\arg\max}\ \frac{\left(\tilde{\mathbf{p}}^T\bar{\mathbf{A}}\tilde{\mathbf{p}}\right)^2}{\tilde{\mathbf{p}}^T\bar{\mathbf{B}}\tilde{\mathbf{p}}\cdot\tilde{\mathbf{p}}^T\tilde{\mathbf{p}}},\end{aligned} \tag{13}$$

where $\bar{\mathbf{A}} := \mathsf{E}_h\left[\mathbf{A}\right]$ and $\bar{\mathbf{B}} := \mathsf{E}_h\left[\mathbf{B}\right]$. Note that the expectation operations in the numerator and denominator are taken independently. Moreover, for the signal term in the numerator, the square of the mean is considered instead of the second moment. This is done to simplify the problem and corresponds to a lower bound of the mean signal power, since $\mathsf{E}_h\left[\tilde{\mathbf{p}}^T\mathbf{A}\tilde{\mathbf{p}}\right]^2 \le \mathsf{E}_h\left[(\tilde{\mathbf{p}}^T\mathbf{A}\tilde{\mathbf{p}})^2\right]$.

Using (18), we obtain for the matrix in the numerator

$$\bar{\mathbf{A}} = \sum_{k=1}^{N} g[N-k]\mathsf{E}_h\left[\mathbf{h}_k\mathbf{h}_k^T\right],$$

where $\mathbf{h}_k^T$ denotes the kth row of $\mathbf{H}$. The matrix $\mathsf{E}_h\left[\mathbf{h}_k\mathbf{h}_k^T\right]$ depends on the mean and covariance of the channel impulse response taps. The (i,j)th-element of the matrix in the denominator computes to

$$\left[\bar{\mathbf{B}}\right]_{i,j} = 4\underbrace{\mathsf{E}_h\left[\mathbf{f}_i^T\mathbf{G}\boldsymbol{\Sigma}_{nn}\mathbf{G}^T\mathbf{f}_j\right]}_{=\mathrm{Tr}\left(\mathbf{G}\boldsymbol{\Sigma}_{nn}\mathbf{G}^T\mathsf{E}_h\left[\mathbf{f}_j\mathbf{f}_i^T\right]\right)} + \begin{cases}\sigma_\gamma^2 & \text{for } i=j\\ 0 & \text{else,}\end{cases}$$

where $\mathbf{f}_i$ is the ith column of $\mathbf{H}$. The optimization problem (13) is of the same form as (6). Compared to the case of full channel knowledge, only the values of the matrices in the numerator and denominator change. Hence, the same optimization algorithm can be used to find the optimized pulse shape, e.g. Newton's method.

For the post-detection filter, the maximization of the mean SINR can be written as

$$\begin{aligned}\mathbf{g}^*_{\text{mSINR}} &= \underset{\mathbf{g}\in\mathbb{R}^N}{\arg\max}\ \frac{\mathsf{E}_h\left[\mathbf{g}^T\mathbf{K}\mathbf{g}\right]}{\mathsf{E}_h\left[\mathbf{g}^T\mathbf{C}\mathbf{g}\right]}\\ &= \mathbf{v}_{\max}\left\{\mathsf{E}_h\left[\mathbf{K}\right], \mathsf{E}_h\left[\tfrac{1}{2}(\mathbf{C}+\mathbf{C}^T)\right]\right\}.\end{aligned} \tag{14}$$

For Gaussian distributed channel taps, the (i,j)th-element of $\bar{\mathbf{K}} = \mathsf{E}_h\left[\mathbf{K}\right]$ is given by

$$\begin{aligned}\left[\bar{\mathbf{K}}\right]_{i,j} =& \mathbf{p}^T\mathsf{E}_h\left[\mathbf{h}_i\mathbf{h}_i^T\right]\mathbf{p}\cdot\mathbf{p}^T\mathsf{E}_h\left[\mathbf{h}_j\mathbf{h}_j^T\right]\mathbf{p}\\ &+ 2\mathbf{p}^T\mathsf{E}_h\left[\mathbf{h}_i\mathbf{h}_j^T\right]\mathbf{p}\cdot\mathbf{p}^T\mathsf{E}_h\left[\mathbf{h}_i\mathbf{h}_j^T\right]\mathbf{p},\end{aligned}$$

[7]The PDF of the energy detector output has been analyzed in detail based on measurements and channel models in [27].

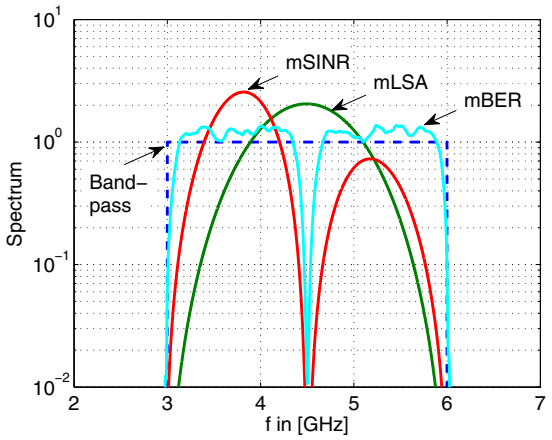

Fig. 4. Spectrum of transmit pulse from different optimization methods with statistical channel knowledge.

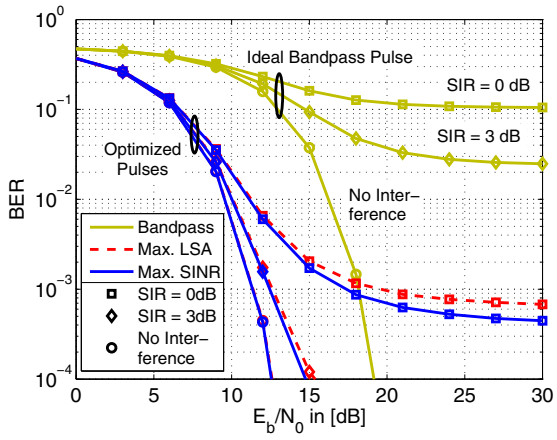

Fig. 5. Performance of transmitter optimization with full channel knowledge.

where $\mathbf{h}_i^T$ is the ith row of $\mathbf{H}$. The expected values of $\mathbf{h}_i\mathbf{h}_j^T$ again depend only on the mean and covariance of the channel impulse response. Likewise, the (i,j)th-element of $\bar{\mathbf{C}} = \mathsf{E}_h\left[\mathbf{C}\right]$ can be written as

$$\left[\bar{\mathbf{C}}\right]_{i,j} = 4\left(\mathbf{p}^T \mathsf{E}_h\left[\mathbf{h}_i\mathbf{h}_j^T\right]\mathbf{p}\right)\left[\mathbf{\Sigma}_{nn}\right]_{i,j} + 4\left[\mathbf{\Sigma}_{nn}\right]_{i,j}^2 - 4\left[\mathbf{\Sigma}_{n'n}\right]_{i,j}^2 .$$

*Maximization of mean Low-*SINR *Approximation (mLSA):* Analogous to the case considered in the previous subsection for full channel knowledge, we perform a low-SINR approximation by neglecting the mixed signal, noise and interference term. This leads to the simplified optimization problem for the transmitter:

$$\mathbf{p}_{\text{mLSA}}^* = \arg\max_{\tilde{\mathbf{p}}\in\mathbb{R}^N} \frac{\tilde{\mathbf{p}}^T\bar{\mathbf{A}}\tilde{\mathbf{p}}}{\tilde{\mathbf{p}}^T\tilde{\mathbf{p}}} = \mathbf{v}_{\max}\left\{\bar{\mathbf{A}}\right\} \tag{15}$$

The denominator is then independent of the pulse shape and does not need to be considered for the optimization. Thus, mLSA corresponds to finding the pulse shape that maximizes the mean of the energy detector output (or, more precisely, the mean of the decision variable z_0) with respect to noise, interference and channel.

Fig. 4 shows the result of a transmitter optimization to compare the three optimization methods mBER, mSINR and mLSA. The spectrum of the transmit pulses is plotted, optimized with statistical channel knowledge and the presence of an interference source at 4.5 GHz. The mBER optimization is based on $M_h = 10^5$ randomly drawn channel realizations. For this example a setting has been chosen[8], which shows the characteristics of the different methods. It can be seen that mBER as well as mSINR place a notch in the spectrum at the frequency of the interferer. The reason for this is to minimize the mixed interference plus noise term β. However, this is not the case for mLSA, since here the mixed term is neglected. The mBER pulse seems to approximate the bandpass pulse and uses almost the whole transmission band with the exception of the interference frequency.

[8]Optimization parameters: $B = 3$ GHz, $f_c = 4.5$ GHz, SIR $= 3$ dB, Gaussian channel taps, exponential PDP with $\sigma_h = 10$ ns, Post-detection filter: First-order low-pass with $f_{\text{cutoff}} = 25$ MHz (as defined in Section V). We used the MATLAB function `fminunc` with the gradient and Hessian as provided in Appendix C and Section IV-B.

V. Performance Evaluation

For the performance evaluation we consider a UWB system with a bandwidth of $B = 3$ GHz at a center frequency of $f_c = 4.5$ GHz. The duration of the PPM half slot is chosen as $T_{\text{ppm}} = 50$ ns. With a duty cycle of 100%, this would correspond to a data rate of 10 Mbps. As figure of merit we consider the BER versus signal-to-noise-ratio, which is defined as E_b/N_0, with E_b denoting the energy per bit and $N_0/2$ the noise power spectral density. We consider a single narrowband interferer with bandwidth $\text{BW}_\text{i} = 10$ MHz at $f_\text{i} = 4.5$ GHz. Simulations show that there is no significant influence of the value of f_i. The power of the interference is measured by the signal-to-interference ratio, which is defined as $\text{SIR} = \frac{P_S}{P_I} = \frac{E_b/T_{\text{symb}}}{I_0\cdot\text{BW}_\text{i}}$, where $I_0/2$ is the power spectral density of the interference in the considered band. The band-pass filter at the receiver input is assumed to be perfectly band limiting for the considered transmission band from 3 to 6 GHz. Hence, the (i,j)th-element of the noise plus interference covariance matrix is given by

$$\left[\mathbf{\Sigma}_{nn}\right]_{i,j} = N_0\tfrac{2B}{f_s}\,\text{sinc}\left(\tfrac{B(i-j)}{f_s}\right)\cos\left(2\pi\tfrac{f_c}{f_s}(i-j)\right) + I_0\tfrac{2\text{BW}_\text{i}}{f_s}\,\text{sinc}\left(\tfrac{\text{BW}_\text{i}(i-j)}{f_s}\right)\cos\left(2\pi\tfrac{f_\text{i}}{f_s}(i-j)\right),$$

with the simulation sampling frequency $f_s = 30$ GHz.

A. Simulation results based on channel model

To evaluate the performance of the proposed optimization schemes in a generic setting, we consider a simple channel model. This channel model assumes that the band-pass filtered channel impulse responses $\tilde{\mathbf{h}}$ are drawn from a Gaussian distribution with zero-mean and covariance matrix $\mathbf{\Sigma}_h$, i.e. $\tilde{\mathbf{h}} \sim \mathcal{N}(\mathbf{0}, \mathbf{\Sigma}_h)$. The channel impulse responses have an exponential PDP with RMS delay spread $\sigma_h = 10$ ns. The channel covariance matrix is given by $\mathbf{\Sigma}_h = \mathbf{F}_{\text{BP}}\mathbf{D}_{\text{pdp}}\mathbf{F}_{\text{BP}}^T$ with $\left[\mathbf{F}_{\text{BP}}\right]_{i,j} = \frac{2B}{f_s}\,\text{sinc}\left(\frac{B(i-j)}{f_s}\right)\cdot\cos\left(2\pi\frac{f_c}{f_s}(i-j)\right)$ and the diagonal PDP matrix $\left[\mathbf{D}_{\text{pdp}}\right]_{i,i} = \frac{1}{\sigma_h}\exp\left(-\frac{i}{f_s\sigma_h}\right)$.

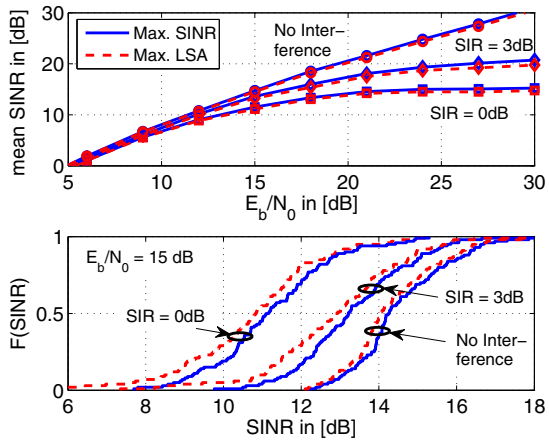

Fig. 6. Transmitter optimization: Mean SINR vs. E_b/N_0 and CDF of SINR for $E_b/N_0 = 15$ dB.

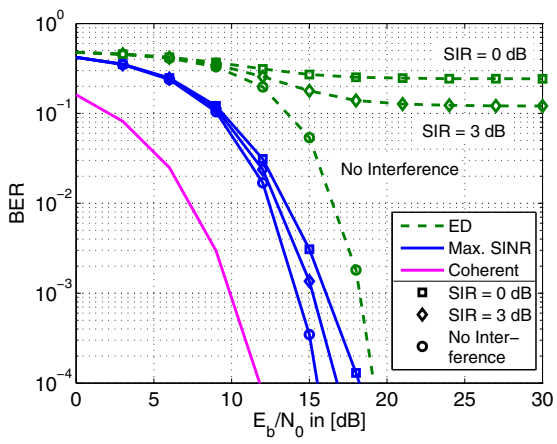

Fig. 7. Performance of receiver optimization with full channel knowledge.

Transmitter Optimization: The optimization results show that the transmitter prefers frequencies where the channel conditions are good. We observe in the magnitudes of the spectrum of the optimized pulses some similarities to the transfer function of the channel. Moreover, the pulses are formed in a way that they suppress the narrowband interference and that they are matched to the post-detection filter. Here, a very low complexity implantation has been chosen with a first-order low-pass filter with impulse response $g[k] = g_0 \exp\left(-\frac{k2\pi f_{\text{cutoff}}}{f_s}\right)$. The cutoff frequency is set to $f_{\text{cutoff}} = 25$ MHz. Fig. 5 shows the mean BER of the transmitter optimization with full channel knowledge for the fixed receiver, averaged over 100 channel realizations. For comparison, the plot depicts the mean BER with an ideal bandpass pulse with perfect synchronization. The dashed lines show the mean BER of the low-SINR approximation (LSA). Markers label different interference levels, i.e. circles, diamonds and squares correspond to the case without interference, SIR $= 3$ dB, and SIR $= 0$ dB, respectively. The plot shows that without interference, more than 6 dB gain can be achieved by the optimized transmitter compared to transmission of an ideal bandpass pulse. Moreover, the precoding can effectively suppress the interference. Whereas for SIR = 0 dB the BER saturates at about 0.1 for the bandpass pulse, the optimized transmission scheme still achieves an acceptable BER of less than 10^{-3}. To compare the SINR maximization with LSA, Fig. 6 shows in the upper plot the mean SINR versus E_b/N_0 for both schemes. The solid and the dashed lines correspond to maximization of SINR and LSA, respectively. It can be seen that the analytical result (lines) according to (3) and the empirically estimated SINR from the simulation (markers) coincide. In low SINR the approximation (LSA) is tight and even in higher SINR the deviation is not large. The lower plot in Fig. 6 shows the CDF of the SINR for $E_b/N_0 = 15$ dB. The dashed line corresponds to LSA and is constantly worse than the SINR maximization.

Receiver Optimization: Fig. 7 shows the performance of the receiver optimization with full channel knowledge for a fixed transmit pulse. Here, just an ideal bandpass pulse has been chosen for transmission. The post-detection filter has been optimized for 4000 channel realizations each. We observe that the optimized $g(t)$ shows similarities to the time-reversed and squared channel impulse response, which would be optimal under a Gaussian assumption. However, the optimized filter can also suppress narrowband interference. The plot shows for comparison the mean BER of a conventional energy detector (ED) with rectangular integration window (dashed line). The length of the integration window is 50 ns. Moreover, the performance is plotted, if a coherent detector would have been used. The coherent receiver is about 3 dB better than the optimized generalized energy detector. The conventional energy detector suffers strongly from narrowband interference. With SIR $= 3$ dB the BER is greater than 10%. The optimization of the post-detection filter achieves small degradation even in presence of strong narrowband interference.

B. Measured Channels

To analyze the performance of the proposed optimization schemes in a real environment, an extensive measurement campaign has been performed. The measurements took place in an indoor rich multipath environment. Fig. 8 shows the floor plan of the room with 22 regions. For each of these regions of size 27 cm $\times$ 56 cm, about 600 channel impulse responses have been measured. With these measurements, the performance of location-aware transmitter and receiver optimization is evaluated for each region. We consider the transmission from the CH to low complexity SNs located in different regions. In the first scenario, the receiver is assumed to be fixed and a region specific pulse shape has been determined. In the second scenario, the low complexity SNs may be able to adjust the post-detection filter. The BER performance for both transmission schemes is determined under the influence of narrowband interference. In this paper, we present the results for two characteristic regions, namely region 9, which is a typical line-of-sight (LOS) situation, and region 17, which is a worst case non-line-of-sight (NLOS) situation.

Transmitter optimization: Fig. 9 and 10 show the mean BER for the first scenario for region 9 and region 17, respectively. The dashed lines show the BER without interference

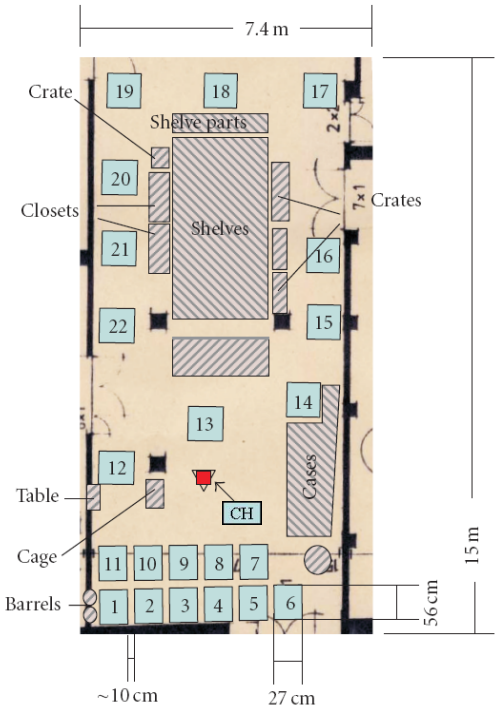

Fig. 8. Floor plan of measurement scenario.

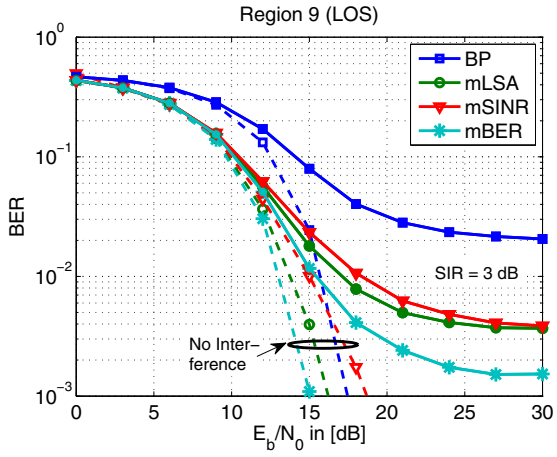

Fig. 9. Performance of transmitter optimization with statistical channel knowledge for a LOS region.

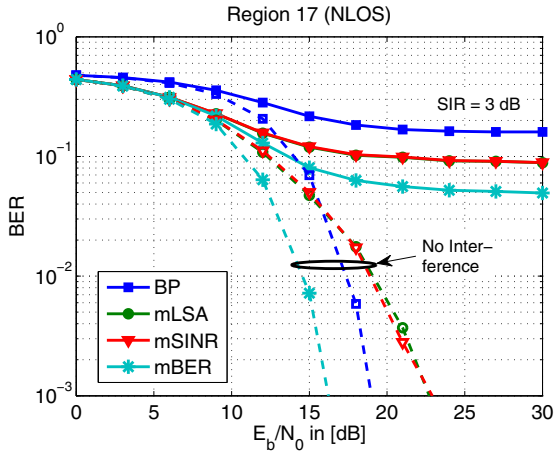

Fig. 10. Performance of transmitter optimization with statistical channel knowledge for a NLOS region.

and the solid lines the case of SIR $= 3$ dB. As a reference, the performance of transmission of an ideal bandpass pulse is plotted (squares). In the LOS situation, the performance is better than in NLOS, because the direct path contains the most energy. Moreover, the channel impulse responses from these regions have more structure, which enables the transmitter optimization to work more effectively. For the case without interference, the mBER pulse (asterisks) is about 2.5 dB better than the bandpass pulse. Narrowband interference can effectively be suppressed leading to 7.5 to 31 % BER reduction for mBER at high SNR for LOS and NLOS, respectively. The mSINR (triangles) and mLSA (circles) optimizations lie in between if E_b/N_0 is not too high. Interestingly, for the LOS region, the low-SINR approximation (mLSA) performs better than mSINR. However, for the LOS region the approximations still show performance gains. For the NLOS case without interference, it can be observed that the approximations perform worse than the simple transmission of a bandpass pulse. This is because especially at high E_b/N_0 the maximization of mean SINR does not minimize the bit error probability. In this case, some bad channel realizations dominate the BER performance, which is not considered by the mean SINR objective function.

Receiver Optimization: Fig. 11 and 12 show the receive filter optimization for region 9 and region 17, respectively. Again, at the transmitter an ideal bandpass pulse is chosen. The plots show the post-detection filter optimization based on the region knowledge (solid lines) as well as with full channel knowledge (dotted lines). Surprisingly, the optimization based on the statistical channel knowledge almost achieves the performance with full channel knowledge and the interference is successfully suppressed. For the NLOS case (Fig. 12), the performance is worse than for the LOS case. The reason for this is that the channel in this regions differ more and have less structure than in the LOS region. However, it can be seen that the regional channel knowledge enables very good detection performance and makes the receiver less vulnerable to narrowband interference compared to conventional energy detection. Moreover, it is robust and only the region where the receiver is located must be known to adapt the post-detection filter.

VI. Implementation Issues and Complexity Analysis

Noncoherent receivers are the key to low cost and low complexity implementations of UWB sensor nodes. Coherent detectors provide a better BER performance but require either very high sampling rates or a high number of rake fingers, which make them impractical for low-power devices. Implementations of noncoherent UWB receivers with energy detection have been shown with a power consumption as low as 136 mW at 5 Mbps data rate (e.g. [29]) or, when applying a low-duty cycle operation, even less than 1 mW (see [8]) for 500 kbps. In this paper, we present two efficient ways

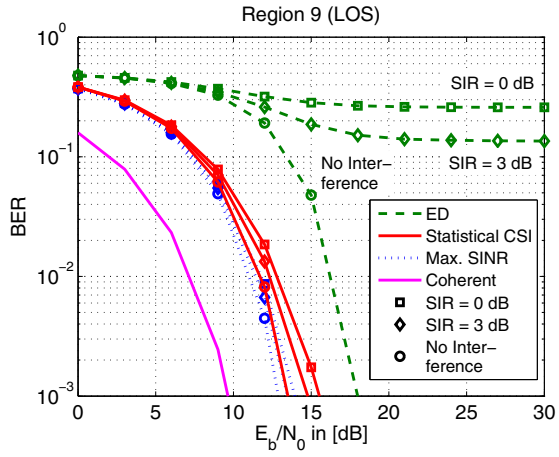

Fig. 11. Performance of receiver optimization with statistical channel knowledge for a LOS region.

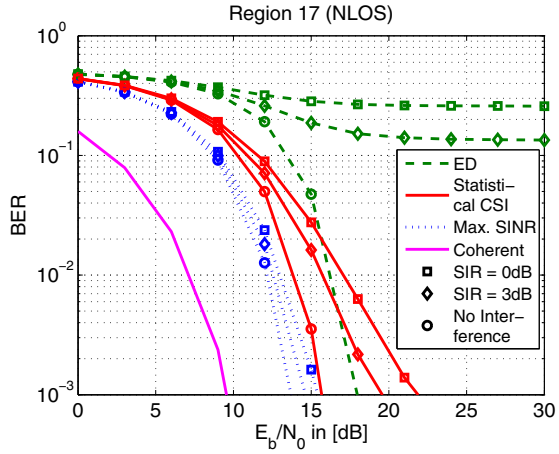

Fig. 12. Performance of receiver optimization with statistical channel knowledge for a NLOS region.

to partially recover the performance loss of energy detection receivers. Both come with little implementation overhead, which is described in the following.

- *Transmitter optimization:* The precoding approach shifts all complexity from the receiver to the transmitter at the CH. Hence, the receiver is not required to adapt to the channel conditions and a fixed post-detection filter can be exploited, e.g. a simple first order low-pass filter. To apply the transmitter optimization, the CH must be able to adapt to the transmit signal. Although this comes with a higher complexity, it is a reasonable assumption since the CH is a full-function device with less stringent constraints on power and cost. Moreover, it is not necessary to perform a convolution with the optimized pulses at the transmitter. The adaptation can be realized with a look-up table with the predetermined pulses. The optimization is based on the location of the SN. Thus, it can be avoided to estimate the channel at the SNs, which would be impractical due to their non-coherent receivers. Instead of the complete channel impulse response, only the region of the SN is needed. The narrowband interference suppression is based on the covariance matrix of the interference. This can be obtained either by a priori knowledge of the coexisting narrowband communication systems or from measurements at the CH. The latter assumes that the CH is exposed to the same interference conditions as the SN, which is reasonable for short range systems.
- *Receiver optimization:* For the implementation of the receiver optimization, the SNs require an adaptable post-detection filter. For an analog implementation, the optimized impulse response can serve as design guideline for the filter and additionally it can be used as a benchmark for implementation. Even a digital implementation of the post-detection filter is favorable in terms of complexity compared to coherent detection. To trade performance for a lower complexity, the post-detection filter can be optimized in a subspace, i.e. using the substitution $\mathbf{g} \mapsto \mathbf{W}\tilde{\mathbf{g}}$, where the columns of $\mathbf{W}$ are the basis vectors of the considered subspace. This enables to restrict the optimization to specific filter structures or to limit the bandwidth or sampling frequency. For location-aware adaption, the SN does not need to estimate the channel. Its location or its region can simply be estimated by the CH and then send to the SN. This saves substantial channel estimation and dissemination overhead.

Location-aware communication requires a database with the mapping of locations to channel statistics. For a stationary environment (as typical for indoor scenarios), this can be build up in a calibration phase from training data. Due to the statistical channel model, the optimization is robust against small changes of the propagation environment. The performance of the precoding depends on the size of the region and on the characteristics of the multipath. A smaller region, and thus better channel knowledge, would lead to better performances. The receiver optimization is more robust to channel uncertainty.

VII. Conclusion

Location information can help to improve the detection performance of low complexity UWB communication. We studied location-aware transmitter and receiver optimizations for generalized energy detection receivers with binary pulse position modulation. The performance evaluation based on measurements shows a 2-5 dB gain compared to simple energy detection. This provides a promising synergy of localization and communication for low complexity UWB sensor networks.

Appendix A
Proof of Proposition 1

First, we compute the numerator of (1). The expectation of (2) yields

$$\mu_\alpha = \mathsf{E}\left[z_0 | a_0 = 0\right] = \mathsf{E}\left[\alpha + \beta + \gamma\right] = \mathsf{E}[\alpha] = \alpha. \qquad (16)$$

The mixed signal and interference plus noise component β is zero mean and the means of the squared interference plus noise components γ cancel out, since the random processes are assumed to be stationary. It follows that

$$\alpha = \mathbf{g}^T(\mathbf{Hp} \odot \mathbf{Hp}) = \sum_{k=1}^{N} g[N-k](\mathbf{p}^T \mathbf{h}_k \mathbf{h}_k^T \mathbf{p}), \qquad (17)$$

where $\mathbf{h}_k^T$ denotes the kth row of $\mathbf{H}$. Expression (17) can be further simplified to

$$\mathbf{p}^T \left(\sum_{k=1}^{N} g[N-k] \mathbf{h}_k \mathbf{h}_k^T \right) \mathbf{p} = \mathbf{p}^T \mathbf{H}^T \mathbf{G} \mathbf{H} \mathbf{p}. \quad (18)$$

For the denominator, the variance of (2) yields

$$\mathsf{Var}[z_0 | a_0 = 0] = \mathsf{E}\left[(z_0 - \mu_\alpha)^2 \right] = \underbrace{\mathsf{E}\left[\beta^2\right]}_{=:\sigma_\beta^2} + \underbrace{\mathsf{E}\left[\gamma^2\right] - \mathsf{E}\left[\gamma\right]^2}_{=:\sigma_\gamma^2}.$$

The second moment of β computes to

$$\begin{aligned} \sigma_\beta^2 &= \mathsf{E}\left[\left(2\mathbf{g}^T (\mathbf{H}\mathbf{p} \odot \mathbf{n}) \right)^2 \right] \\ &= 4\mathsf{E}\left[((\mathbf{G}\mathbf{n})^T \mathbf{H}\mathbf{p})^2 \right] \\ &= \mathbf{p}^T 4\mathbf{H}^T \mathbf{G} \underbrace{\mathsf{E}\left[\mathbf{n}\mathbf{n}^T\right]}_{=\mathbf{\Sigma}_{nn}} \mathbf{G}^T \mathbf{H}\mathbf{p}. \end{aligned}$$

With $\mathsf{E}[\gamma] = 0$ follows for the squared interference plus noise term

$$\begin{aligned} \sigma_\gamma^2 &= \mathsf{E}\left[\left(\mathbf{g}^T (\mathbf{n} \odot \mathbf{n}) \right)^2 - 2\mathbf{g}^T (\mathbf{n} \odot \mathbf{n}) \mathbf{g}^T (\mathbf{n}' \odot \mathbf{n}') \right] \\ &\qquad + \mathsf{E}\left[\left(\mathbf{g}^T (\mathbf{n}' \odot \mathbf{n}') \right)^2 \right] \\ &= 2\mathbf{g}^T \mathsf{E}\left[(\mathbf{n} \odot \mathbf{n})(\mathbf{n} \odot \mathbf{n})^T \right] \mathbf{g} \\ &\qquad - 2\mathbf{g}^T \mathsf{E}\left[(\mathbf{n} \odot \mathbf{n})(\mathbf{n}' \odot \mathbf{n}')^T \right] \mathbf{g} \\ &= 4\mathbf{g}^T \left(\mathbf{\Sigma}_{nn} \odot \mathbf{\Sigma}_{nn} - \mathbf{\Sigma}_{n'n} \odot \mathbf{\Sigma}_{n'n} \right) \mathbf{g}. \end{aligned} \quad (19)$$

The last line follows from the property of the zero mean multivariate normal distribution $\mathsf{E}\left[n_i^2 n_j^2\right] = 2\mathsf{E}\left[n_i n_j\right]^2 + \mathsf{E}\left[n_i^2\right]\mathsf{E}\left[n_j^2\right]$, where n_i and n_j denotes the ith and jth element of the vector $\mathbf{n}$, respectively [30]. Collecting terms and substitution of $\mathbf{A}$ and $\mathbf{B}_\beta$ yields finally (3). ∎

APPENDIX B
PROOF OF PROPOSITION 2

With (16) we obtain for the numerator of (1)

$$\mu_\alpha^2 = \left(\mathbf{g}^T (\mathbf{q} \odot \mathbf{q}) \right)^2 = \mathbf{g}^T \left(\mathbf{H}\mathbf{p}\mathbf{p}^T \mathbf{H}^T \odot \mathbf{H}\mathbf{p}\mathbf{p}^T \mathbf{H}^T \right) \mathbf{g}.$$

For the denominator of (1), we note that σ_β^2 can be written in terms of $\mathbf{g}$ as

$$\begin{aligned} \sigma_\beta^2 &= 4\mathsf{E}\left[\left(\mathbf{g}^T (\mathbf{q} \odot \mathbf{n}) \right)^2 \right] \\ &= 4\mathbf{g}^T \mathsf{E}\left[(\mathbf{q} \odot \mathbf{n})(\mathbf{q} \odot \mathbf{n})^T \right] \mathbf{g} \\ &= 4\mathbf{g}^T \left(\mathbf{q}\mathbf{q}^T \odot \mathsf{E}\left[\mathbf{n}\mathbf{n}^T\right] \right) \mathbf{g} \\ &= \mathbf{g}^T \left(4\mathbf{H}\mathbf{p}\mathbf{p}^T \mathbf{H}^T \odot \mathbf{\Sigma}_{nn} \right) \mathbf{g}. \end{aligned}$$

With σ_γ^2 as given in (19) follows directly (4). ∎

APPENDIX C
GRADIENT AND HESSIAN MATRIX FOR SINR OPTIMIZATION

For transmitter optimization, the objective function can be written as

$$\mathrm{SINR} = \frac{\left(\tilde{\mathbf{p}}^T \mathbf{A} \tilde{\mathbf{p}} \right)^2}{\tilde{\mathbf{p}}^T \mathbf{B} \tilde{\mathbf{p}} \cdot \tilde{\mathbf{p}}^T \tilde{\mathbf{p}}} = \frac{s^2}{n \cdot c},$$

where $s := \tilde{\mathbf{p}}^T \mathbf{A} \tilde{\mathbf{p}}$, $n := \tilde{\mathbf{p}}^T \mathbf{B} \tilde{\mathbf{p}}$ and $c := \tilde{\mathbf{p}}^T \tilde{\mathbf{p}}$. The gradient with respect to $\tilde{\mathbf{p}}$ is given by

$$\nabla_{\tilde{\mathbf{p}}} \mathrm{SINR} = \frac{2s}{n \cdot c} \nabla s - \frac{s^2}{(n \cdot c)^2} (c \nabla n + n \nabla c)$$

where $\nabla s = 2\mathbf{A}\tilde{\mathbf{p}}$, $\nabla n = 2\mathbf{B}\tilde{\mathbf{p}}$ and $\nabla c = 2\tilde{\mathbf{p}}$. The Hessian matrix with respect to $\tilde{\mathbf{p}}$ is given by

$$\begin{aligned} H_{\tilde{\mathbf{p}}}\, \mathrm{SINR} = \mathbf{v}_1 (\nabla s)^T - \mathbf{v}_2 (\nabla n)^T - \mathbf{v}_3 (\nabla c)^T \\ + \frac{2s}{n \cdot c} 2\mathbf{A} - \frac{s^2}{n^2 \cdot c} 2\mathbf{B} - \frac{s^2}{n \cdot c^2} 2\mathbf{I}, \end{aligned}$$

where

$$\begin{aligned} \mathbf{v}_1 &= \frac{2}{nc} \nabla s - \frac{2s}{(nc)^2} (c \nabla n + n \nabla c), \\ \mathbf{v}_2 &= \frac{2s}{n^2 c} \nabla s - \frac{s^2}{(n^2 c)^2} \left(c \cdot 2n \nabla n + n^2 \nabla c \right), \\ \mathbf{v}_3 &= \frac{2s}{c^2 n} \nabla s - \frac{s^2}{(c^2 n)^2} \left(c^2 \nabla n + n \cdot 2c \nabla c \right). \end{aligned}$$

For receiver optimization, the gradient of the SINR with respect to $\mathbf{g}$ computes to

$$\nabla_{\mathbf{g}} \mathrm{SINR} = \frac{1}{\mathbf{g}^T \mathbf{C} \mathbf{g}} 2\mathbf{K}\mathbf{g} - \frac{\mathbf{g}^T \mathbf{K} \mathbf{g}}{\left(\mathbf{g}^T \mathbf{C} \mathbf{g} \right)^2} (\mathbf{C} + \mathbf{C}^T) \mathbf{g},$$

and the Hessian matrix to

$$\begin{aligned} H_{\mathbf{g}}\, \mathrm{SINR} = &\mathbf{w}_1 (2\mathbf{K}\mathbf{g})^T - \mathbf{w}_2 ((\mathbf{C} + \mathbf{C}^T)\mathbf{g})^T \\ &+ \frac{1}{\mathbf{g}^T \mathbf{C} \mathbf{g}} 2\mathbf{K} - \frac{\mathbf{g}^T \mathbf{K} \mathbf{g}}{\left(\mathbf{g}^T \mathbf{C} \mathbf{g} \right)^2} (\mathbf{C} + \mathbf{C}^T), \end{aligned}$$

where

$$\begin{aligned} \mathbf{w}_1 &= \frac{-1}{(\mathbf{g}^T \mathbf{C} \mathbf{g})^2} (\mathbf{C} + \mathbf{C}^T) \mathbf{g} \\ \mathbf{w}_2 &= \frac{1}{(\mathbf{g}^T \mathbf{C} \mathbf{g})^2} 2\mathbf{K}\mathbf{g} - \frac{2\mathbf{g}^T \mathbf{K} \mathbf{g}}{\left(\mathbf{g}^T \mathbf{C} \mathbf{g} \right)^3} (\mathbf{C} + \mathbf{C}^T) \mathbf{g}. \end{aligned}$$

REFERENCES

[1] Y. Xu, J. Heidemann, and D. Estrin, "Geography-informed energy conservation for ad hoc routing," in *Proc. 2001 ACM MobiCom*, pp. 70–84.

[2] D. Huang, M. Mehta, D. Medhi, and L. Harn, "Location-aware key management scheme for wireless sensor networks," in *Proc. 2004 ACM SASN*, pp. 29–42.

[3] J. Zhang, P. Orlik, Z. Sahinoglu, A. Molisch, and P. Kinney, "UWB systems for wireless sensor networks," *Proc. IEEE*, vol. 97, no. 2, pp. 313–331, Feb. 2009.

[4] H. Cao, V. Leung, C. Chow, and H. Chan, "Enabling technologies for wireless body area networks: a survey and outlook," *IEEE Commun. Mag.*, vol. 47, no. 12, pp. 84–93, Dec. 2009.

[5] M. G. Di Benedetto, T. Kaiser, A. F. Molisch, I. Oppermann, C. Politano, and D. Porcino, *UWB Communication Systems–A Comprehensive Overview*. Hindawi Publishing Corporation, 2006.

[6] K. Witrisal, G. Leus, G. Janssen, M. Pausini, F. Troesch, T. Zasowski, and J. Romme, "Noncoherent ultra-wideband systems," *IEEE Signal Process. Mag.*, vol. 26, no. 4, pp. 48–66, July 2009.

[7] C. Steiner, F. Althaus, F. Trösch, and A. Wittneben, "Ultra-wideband geo-regioning: a novel clustering and localization technique," *EURASIP J. Adv. Signal Process.*, Nov. 2007.

[8] F. Troesch, C. Steiner, T. Zasowski, T. Burger, and A. Wittneben, "Hardware aware optimization of an ultra low power UWB communication system," in *Proc. 2007 IEEE Int. Conf. Ultra-Wideband*, pp. 174–179.

[9] C. Steiner and A. Wittneben, "Cognitive interference suppression for low complexity UWB transceivers," in *Proc. 2008 IEEE Int. Conf. Ultra-Wideband*.

[10] H. Luecken, T. Zasowski, C. Steiner, F. Troesch, and A. Wittneben, "Location-aware adaptation and precoding for low complexity IR-UWB receivers," in *Proc. 2008 IEEE Int. Conf. Ultra-Wideband*, pp. 31–34.
[11] X. Luo, L. Yang, and G. Giannakis, "Designing optimal pulse-shapers for ultra-wideband radios," *J. Commun. Netw.*, vol. 5, no. 4, pp. 344–353, Dec. 2003.
[12] B. Hu and N. Beaulieu, "Pulse shapes for ultrawideband communication systems," *IEEE Trans. Wireless Commun.*, vol. 4, no. 4, pp. 1789–1797, July 2005.
[13] Y. Zhu and H. Wu, "Integrated distributed transversal filters for pulse shaping and interference suppression in UWB impulse radios," in *Proc. 2006 IEEE Int. Conf. Ultra-Wideband*.
[14] T. Strohmer, M. Emami, J. Hansen, G. Papanicolaou, and A. Paulraj, "Application of time-reversal with MMSE equalizer to UWB communications," in *Proc. 2004 IEEE Global Telecommun. Conf.*, vol. 5, pp. 3123–3127.
[15] H. T. Nguyen, I. Kovacs, and P. Eggers, "A time reversal transmission approach for multiuser UWB communications," *IEEE Trans. Antennas Propag.*, vol. 54, no. 11, pp. 3216–3224, Nov. 2006.
[16] N. Guo, B. Sadler, and R. Qiu, "Reduced-complexity UWB time-reversal techniques and experimental results," *IEEE Trans. Wireless Commun.*, vol. 6, no. 12, pp. 4221–4226, Dec. 2007.
[17] Y.-H. Chang, S.-H. Tsai, X. Yu, and C.-C. Kuo, "Performance enhancement of channel-phase precoded ultra-wideband (CPP-UWB) systems by rake receivers," in *Proc. 2008 IEEE Global Telecommun. Conf.*
[18] ——, "Codeword design for ultra-wideband (UWB) precoding," *IEEE Trans. Wireless Commun.*, vol. 9, no. 1, pp. 198–207, Jan. 2010.
[19] A.-H. Mohsenian-Rad, J. Mietzner, R. Schober, and V. Wong, "Pre-equalization for pre-rake DS-UWB systems with spectral mask constraints," *IEEE Trans. Commun.*, vol. 59, no. 3, pp. 780–791, Mar. 2011.
[20] M. Weisenhorn and W. Hirt, "ML receiver for pulsed UWB signals and partial channel state information," in *Proc. 2005 IEEE Int. Conf. Ultra-Wideband*, pp. 379–384.
[21] A. D'Amico, U. Mengali, and E. Arias-de Reyna, "Energy-detection UWB receivers with multiple energy measurements," *IEEE Trans. Wireless Commun.*, vol. 6, no. 7, pp. 2652–2659, July 2007.
[22] T. Zasowski, F. Troesch, and A. Wittneben, "Partial channel state information and intersymbol interference in low complexity UWB PPM detection," in *Proc. 2006 IEEE Int. Conf. Ultra-Wideband*, pp. 369–374.
[23] T. Zasowski and A. Wittneben, "Performance of UWB receivers with partial CSI using a simple body area network channel model," *IEEE J. Sel. Areas Commun.*, vol. 27, no. 1, pp. 17–26, Jan. 2009.
[24] H. Luecken, C. Steiner, and A. Wittneben, "ML timing estimation for generalized UWB-IR energy detection receivers," in *Proc. 2009 IEEE Int. Conf. Ultra-Wideband*, pp. 829–833.
[25] FCC, "Revision of part 15 of the commission's rules regarding ultra-wideband transmission systems," 1st Report and Order, ET Docket 98-153, FCC 02-48, adopted/released Feb. 14/Apr. 22 2002.
[26] R. Horn and C. Johnson, *Matrix Analysis*. Cambridge University Press, 1985.
[27] C. Steiner and A. Wittneben, "Low complexity location fingerprinting with generalized UWB energy detection receivers," *IEEE Trans. Signal Process.*, vol. 58, no. 3, pp. 1756–1767, Mar. 2010.
[28] S. Dubouloz, B. Denis, S. de Rivaz, and L. Ouvry, "Performance analysis of LDR UWB non-coherent receivers in multipath environments," in *Proc. 2005 IEEE Int. Conf. Ultra-Wideband*, pp. 491–496.
[29] L. Stoica, A. Rabbachin, H. Repo, T. Tiuraniemi, and I. Oppermann, "An ultrawideband system architecture for tag based wireless sensor networks," *IEEE Trans. Veh. Technol.*, vol. 54, no. 5, pp. 1632–1645, Sep. 2005.
[30] L. Isserlis, "On a formula for the product-moment coefficient of any order of a normal frequency distribution in any number of variables," *Biometrika*, vol. 12, no. 1-2, pp. 134–139, 1918.

Heinrich Luecken received the Dipl.-Ing. degree in electrical engineering from RWTH Aachen University, Germany, in 2007. Since October 2007, he is with the Communication Technology Laboratory at the Swiss Federal Institute of Technology (ETH) Zurich, Switzerland, working towards the Ph.D. degree. His research interests include signal processing for Ultra-Wideband communication, localization, and imaging.

Christoph Steiner received the Dipl.-Ing. degree in telematics from Graz University of Technology, Austria, in 2005 with distinction, and the Ph.D. degree in electrical engineering from the Swiss Federal Institute of Technology (ETH) Zurich in 2010. Since October 2010 he is with Infineon Technologies Austria AG. His research interests are in the field of signal processing for wireless communication and position location.

Armin Wittneben received his MSc and PhD degrees in Electrical Engineering from the Technical University of Darmstadt, Germany, in 1983 and 1989 respectively. In 1989 he joined the central research unit ASCOM Tech of ASCOM Ltd., Switzerland, as postdoctoral researcher. In 1992 he became head of the Wireless Technology and Security Department. In 1996 he also served as co-director of ASCOM Tech. In 1997 he received the Venia Legendi (Habilitation) in Communication Technology from the TU-Darmstadt. In 1998 he accepted a position as full professor of Telecommunication at the Saarland University, Germany. Since 2002 he has been full professor of Wireless Technology at ETH Zurich, Switzerland and is serving as head of the Communication Technology Laboratory. His research interests include all aspects of wireless communication with special emphasis on communication theory, signal processing, cooperative wireless signaling and protocols, distributed MIMO systems and Ultra-Wideband/Ultra-Low Power communication, imaging and position location.